Nonlinear Dynamics (2026) 114:726
https://doi.org/10.1007/s11071-026-12614-5

RESEARCH

Quasineutral invariant manifolds in a nonlinear mathematical model of phage–bacteria interactions *in vitro*

Jesús Ait Idir[1] · Fatima Drubi[1] · Marcos Rodríguez[2] · Irene Cantallops[2] · Pilar Domingo-Calap[2] · Josep Sardanyés[3,4]

Received: 7 January 2026 / Revised: 25 March 2026 / Accepted: 26 April 2026 / Published online: 18 May 2026

Abstract

We analyze a nonlinear system of ordinary differential equations modeling phage–bacteria dynamics in the presence of phage-resistant bacterial strains. The model, calibrated using experimental data for *Klebsiella pneumoniae* and a lytic bacteriophage, describes interactions among susceptible bacteria, infected bacteria, resistant mutants, and free phages under logistic growth constraints. We provide a complete characterization of the equilibria and their stability, showing that the system admits a degenerate normally hyperbolic invariant manifold consisting of a quasineutral line of equilibria. This line is composed of stable and unstable segments whose stability is governed by transverse hyperbolic directions. We show that coexistence between phage-resistant bacteria and phages is organized by this quasineutral manifold, leading to nonhyperbolic asymptotic dynamics with sensitivity to initial conditions. By varying the death rate of resistant bacteria, we identify a global transcritical bifurcation involving an entire continuum of equilibria, resulting in an exchange of stability between two invariant half-lines. This bifurcation provides a rigorous mechanism for the transition between persistence and clearance of phage-resistant bacteria. We further support the analytical results with numerical simulations and a sensitivity analysis based on variational equations, demonstrating the robustness of the observed dynamics. Our results highlight how degenerate invariant manifolds can govern long-term behavior in biologically motivated dynamical systems and provide a mathematically grounded framework for understanding coexistence and elimination scenarios in phage–bacteria interactions.

Keywords Dynamical systems · Global bifurcations · Multidrug-resistant bacteria · Phage-bacteria interactions · Systems biology

Author summary

Bacteriophages–viruses that infect bacteria–are being reconsidered as alternatives to antibiotics, but bacterial resistance to phages often emerges rapidly. Understanding when phages and bacteria coexist and how resistant bacteria can be eliminated remains a major challenge. In this study, we analyze a mathematical model calibrated with *in vitro* data describing interactions between bacteria, bacteriophages, and phage-resistant mutants. Using tools from dynamical systems theory, we show that coexistence between phages and resistant bacteria is organized by a quasineutral line of equilibrium states rather than a single stable equilibrium. This structure explains why long-term dynamics can be highly sensitive to initial conditions without being chaotic. We further identify a bifurcation that leads to the extinction of resistant bacteria when their effective mortality exceeds a critical threshold. Our results provide a mechanistic framework for interpreting resistance-driven outcomes in phage–bacteria systems and highlight how mathematical structure can constrain therapeutic strategies, even in simple experimental settings.

✉ Josep Sardanyés
jsardanyes@crm.cat

[1] Department of Mathematics, University of Oviedo, C. Leopoldo Calvo Sotelo 18, 33007 Oviedo, Spain

[2] Institute for Integrative Systems Biology (I2SysBio), University of Valencia-Consejo Superior de Investigaciones Cientificas (CSIC), C. Catedr/'atic Agust/'in Escardino Benlloch, 46980 Paterna, Val/'encia, Spain

[3] Centre de Recerca Matemática (CRM), Edifici C. Campus de Bellaterra, 08193 Cerdanyola del Vallés, Barcelona, Spain

[4] Dynamical Systems and Computational Virology (CRM - CSIC Associated Unit), Edifici C. Campus de Bellaterra, 08193 Cerdanyola del Vallés, Barcelona, Spain

1 Introduction

The emergence of multidrug-resistant (MDR) bacteria is a mounting global health emergency, threatening the effectiveness of standard antibiotics in facing bacterial infections. According to the World Health Organization, antibiotic resistance is among the top 10 global public health threats. In 2021, 4.71 million (95% with uncertainty interval (UI) 4.23–5.19) deaths were associated with antimicrobial-resistant bacteria, including 1.14 million (95% UI 1.00–1.28) deaths attributable to bacterial resistance [1]. The problem is particularly acute in hospital settings, where MDR strains of, e.g., *Klebsiella pneumoniae*, *Acinetobacter baumannii*, *Pseudomonas aeruginosa*, and *Escherichia coli* are responsible for a growing number of healthcare-associated infections. These pathogens contribute, among others, to extended hospital stays, increased treatment costs, and higher morbidity and mortality [35]. Moreover, the pipeline for new antibiotics remains critically underfunded and insufficient, with few novel agents addressing the most resistant Gram-negative bacteria [17]. This confluence of rising resistance and declining innovation underscores the urgent need for alternative antimicrobial strategies.

Bacteriophages, or phages –viruses that infect and lyse bacteria– are being revisited as a viable therapeutic option in the post-antibiotic era [43]. Unlike broad-spectrum antibiotics, phages are able to amplify and spread locally, targeting microbial pathogens while also being highly specific to their bacterial hosts, minimizing off-target effects on the microbiota [36]. Phage therapy (see Ref. [21] for a recent review), first proposed nearly a century ago, was soon overshadowed by the success of antibiotics. However, the rise of MDR bacteria due to the misuse and overuse of antibiotics is renewing interest in phage therapy as a viable strategy to combat pathogenic bacterial infections. Advances in high-throughput sequencing, metagenomics, genetic engineering, and synthetic biology are now overcoming previous limitations, spurring increased support from funding agencies, biotech startups, and pharmaceutical companies. Recent studies and clinical trials have demonstrated the effectiveness of phage therapy in treating antibiotic-resistant infections, including chronic wound infections, sepsis, and respiratory tract infections caused by *Pseudomonas*, *Staphylococcus*, and *Acinetobacter* species [6, 10, 11, 13, 19, 42]. The adaptability of phages, their natural presence in diverse ecosystems, and their potential for genetic engineering also make them attractive tools for precision medicine and infection control. Phage cocktails and engineered phages are already being explored to broaden host range and prevent the rapid emergence of bacterial resistance during therapy [27, 35].

Effective implementations of phage therapy require a deep understanding of phage-bacteria-host population and co-evolutionary dynamics, and this is where mathematical modeling becomes useful. Models can help predict the dynamics arising from ecological and evolutionary processes between phages and bacteria within the host, thereby enabling better-informed treatment designs [27]. These models can simulate the timing, dosage, and combination strategies needed for phage administration and assess synergies with antibiotics or host immune responses. Furthermore, modeling is crucial for anticipating resistance development and for designing robust phage cocktails tailored to individual infections [35]. As precision medicine continues to evolve, integrating mathematical frameworks into phage therapy protocols will be key to optimizing outcomes and mitigating the global threat of MDR bacteria.

Quantitative mathematical approaches are essential for understanding the complex dynamics of phage-bacteria interactions, particularly in simplified systems. In this context, *in vitro* experiments with MDR strains and phages provide a controlled setting to dissect key interactions and quantify the rates at which key processes occur. By means of mathematical modeling, dynamical systems theory, and statistical methods, researchers can estimate key parameters that control the population dynamics from these experimental data, such as infection rates, burst sizes, or bacterial growth [37]. These quantitative insights can enable more precise predictions of system behavior under various conditions, including different parameter values and initial conditions (i.e., monostable vs. bistable dynamics), shed light on the design of effective phage therapies, and enhance our ability to manipulate microbial ecosystems.

In this direction, a recent work by Rodríguez et al. [37] introduced a mathematical model to analyze the *in vitro* dynamics between *K. pneumoniae* and the lytic phage vB_Kpn_2-P4. Through bacteria growth experiments and mathematical modeling, the authors estimated key population parameters, including bacterial growth rates, phage infection rates, burst sizes, and phage-resistance emergence probabilities. Logistic and nonlinear models were fitted using both Levenberg-Marquardt and Bayesian inference methods, yielding consistent estimates. Results showed that resistant mutants emerged rapidly and grew at rates comparable to the wild-type strain, with minimal fitness cost. These findings highlight the critical role of resistance in shaping phage therapy outcomes and the importance of integrating experimental data with quantitative models to predict and optimize potential therapeutic strategies.

In this manuscript, we analyze the qualitative dynamics of the mathematical model used in the experimental setting described in Ref. [37] (see also Fig. 1). We study the equilibria and the bifurcations, showing a coexistence scenario between phage-resistant bacteria and phages governed by a quasineutral line of equilibria (i.e., a degenerate normally hyperbolic invariant manifold, see Refs. [18, 29, 41] for other

examples of quasineutral manifolds in biological models). Clearance of resistant bacteria is achievable by combining phage treatment with increased degradation of resistant strains, leading to a global transcritical bifurcation. These results highlight the potential of combined phage-antibiotic therapies to clear phage-resistant bacterial populations.

Despite extensive experimental and modeling work on phage–bacteria systems, the dynamical structures governing long-term coexistence and clearance remain poorly characterized. In particular, little attention has been paid to the role of non-hyperbolic invariant sets–such as lines of equilibria–in shaping resistance-driven outcomes. Here, we address this gap by providing a rigorous dynamical systems analysis of a data-calibrated phage–bacteria model, revealing how quasineutral manifolds can organize coexistence, shape sensitivity to initial conditions, and govern clearance transitions.

2 Summary of the experimental results

The selected strain of *Klebsiella pneumoniae* was Kpn63, a clinical strain that belongs to the capsular type KL-64 [17]. This strain harbors a New Delhi metallo-beta-lactamase-1 (NDM-1) enzyme that confers resistance to all beta-lactam antibiotics, including carbapenems. The growth of Kpn63 was monitored without and with the presence of phage vB_Kpn_2-P4 [37]. This is a lytic phage of *K. pneumoniae* isolated from sewage water [17]. The phage vB_Kpn_2-P4 was selected for our study due to its broadest host range in clinical strains of *K. pneumoniae* with capsular type KL-64.

The starting aliquot of the phage vB_Kpn_2-P4 was stored at -80°C in SM buffer and then amplified in Luria-Bertani media supplemented with $CaCl_2$ in the same bacterial strain in which it was isolated to obtain high-titer lysates. Negative (only LB media) and positive (Kpn63 without phage) controls were used to check the efficacy of phage infection. The total volume was passed through a 0.22 μ m filtration unit and concentrated using CP Select InnovaPrep equipment. To determine the number of phage particles in our concentrated aliquots (phage titration), we followed the double-layer agar method. We mixed 10 μL of phage serial dilutions and 100 μL of fresh Kpn63 bacterial cultures in 3.5 mL of liquid top agar at 55°C and plated after vortexing in LB agar plates. After overnight incubation at 37°C, plaque-forming units (PFUs) were counted, reaching a final titer of 1.5×10^{10} PFU mL^{-1}. The appearance of the plaques was small and cloudy; the turbidity of the halos can result from partial bacterial lysis or the activity of phage-associated enzymes (depolymerase), which degrade components of the bacterial cell wall or extracellular matrix without lysing the bacteria.

To study the infectivity of the phage and the phage-bacteria dynamics in liquid medium, we determined the strength of lysis based on time-lapse turbidity (OD_{600}) measurements at 10-min intervals. Our experiments were performed in 96-well plates, incubated at 37°C inside a plate reader (Multiskan) for 16.5 h. Once we knew the correlation of CFU mL^{-1} from our bacterial suspensions and PFU mL^{-1} from the phage aliquots, we tested different initial multiplicity of infection (MOI) conditions by combining 150 μL of bacterial suspension and 10 μL of phage dilution in each well. All experiments were performed with 24 independent replicates per condition (MOI 1, 0.1, 0.01, and 0.001).

3 Mathematical model

In this section we introduce the mathematical model describing the bacteria-phage dynamics used in the experiments carried out in Ref. [37]. Since the experiments were done in a liquid medium, a mean field model based on ordinary differential equations (ODEs), i.e., the limit of infinite diffusion, was used. The state variables of the model are the density of wild-type (wt) *Klebsiella* strains $y(t)$, infected *Klebsiella* strains $y_f(t)$, phages $\phi(t)$, and phage-resistant *Klebsiella* strains $x(t)$.

The variable x may be either considered as a single type of phage-resistant mutant or as an average population of different resistant mutants. The key modeled processes, shown in Fig. 2(b), can be represented by the following stoichiometric relations, being s the available nutrients, which are not explicitly considered:

$$y + s \xrightarrow{k(1-\mu)} y + y, \tag{1}$$
$$y + s \xrightarrow{k\mu} y + x, \tag{2}$$
$$y + \phi \xrightarrow{\rho} y_f, \tag{3}$$
$$y_f \xrightarrow{\eta} \varnothing, \tag{4}$$
$$y_f \xrightarrow{\eta} \beta\,\phi, \tag{5}$$
$$x + s \xrightarrow{\gamma} x + x, \tag{6}$$
$$x \xrightarrow{\epsilon} \varnothing, \tag{7}$$

Reaction (1) is the duplication of *Klebsiella* wt cells (by consumption of nutrients s) and is proportional to the intrinsic growth rate $k > 0$, with $\mu \in [0, 1]$ being the probability of producing a resistant strain. Notice we assume in reaction (2) that resistant strains arise due to mutations during wt replication. Reaction (3) is the infection of wt cells, which is proportional to the infection rate $\rho > 0$. Infected cells die due to lysis by phages at a rate $\eta > 0$, where $\beta \gg 1$ denotes the burst size (i.e., the number of phages released upon lysis), see reactions (4)-(5). Phage-resistant cells duplicate at a rate $\gamma > 0$ [reaction (6)] and they die at a rate $\epsilon > 0$ [reaction (7)]. The above set of reactions can be modeled using

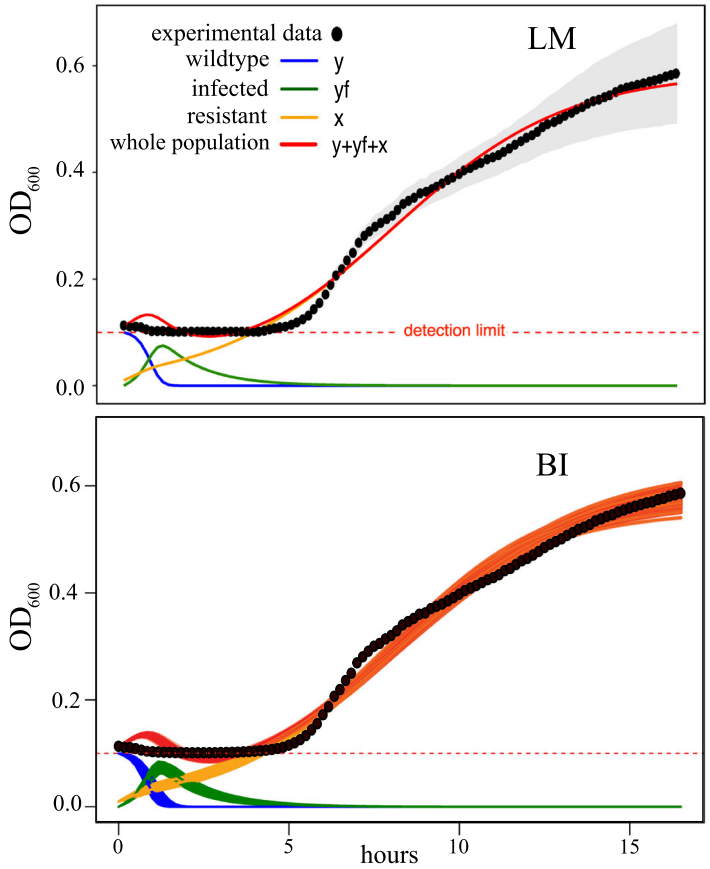

Levenberg-Marquardt (LM)

Parameter	Value	SE
μ	0.5544	2.042e-03
ρ	0.9625	1.556e-04
η	0.7879	1.514e-04
ε	0.1915	9.358e-03
β	225.8021	4.878e-02
γ	0.5788	1.300e-02

Bayesian inference (BI)

Parameter	Value	SE
μ	0.4449	8.83e-02
ρ	0.9359	4.16e-02
η	0.8452	6.78e-02
ε	0.1904	2.45e-02
β	170.4271	2.99e+01
γ	0.5794	4.24e-02
sdlog.N	0.0984	7.46e-03

Fig. 1 Model fit to the experimental data and parameter estimation. (Left) Dynamics of wild-type (wt) *Klebsiella pneumoniae* in the presence of the bacteriophage vB_Kpn_2-P4 monitored *in vitro* (black dots). Bacterial densities are measured with the optical density (OD_{600}). The dynamics obtained with the mathematical model given by Eqs. (8)-(11) and fit to the data are shown: wt population (y, blue lines); infected bacteria (y_f, green lines); resistant bacteria (x, orange lines). The sum of all the bacterial populations (red lines) was used to compare with the experimental data. Notice that the orange lines appeared overlapped with the red ones when the phage-resistant bacteria out-competed the other strains. Fits were done with the mean populations from the experiments averaged over 21 independent replicas using two methods: the Levenberg-Marquardt (LM) and Bayesian inference (BI). (Right) Estimated parameter values using the LM and BI, with an intrinsic growth rate of the wt bacteria of $k = 0.538$ and with carrying capacity (expressed as OD) $C = 0.887$. These two latter values were obtained for *K. pneumoniae* dynamics alone (see Ref. [37] for details). See Table 1 for a detailed description of the model parameters

the Law of Mass Action, giving rise to a dynamical system governed by the following set of ODEs:

$$\frac{dy}{dt} = k\,(1-\mu)\,y\,\omega(y,x) - \rho\,y\,\phi, \tag{8}$$

$$\frac{dy_f}{dt} = \rho\,y\,\phi - \eta\,y_f, \tag{9}$$

$$\frac{dx}{dt} = (k\,\mu\,y + \gamma\,x)\,\omega(y,x) - \varepsilon\,x, \tag{10}$$

$$\frac{d\phi}{dt} = \beta\,\eta\,y_f - \rho\,y\,\phi, \tag{11}$$

where the function

$$\omega(y,x) = 1 - \frac{y+x}{C}, \tag{12}$$

is a logistic growth constraint including competition between the bacterial strains that duplicate. In this paper, we consider both df/dt and $\dot{f}$ as valid notation for the first derivative.

Several modeling assumptions deserve comment. We neglect superinfection of already infected cells and explicit phage decay, assumptions justified by the short experimental time scales and the large burst sizes observed in vitro. The decay term for phage-resistant bacteria represents an effective mortality that may arise from fitness costs, immune-mediated clearance, or synergistic antibiotic effects. Importantly, the qualitative dynamics reported here do not depend on the specific biological origin of this term, but rather on its magnitude relative to the growth rate of the resistant population.

The model further assumes that infected bacteria do not proliferate and therefore do not compete for nutri-

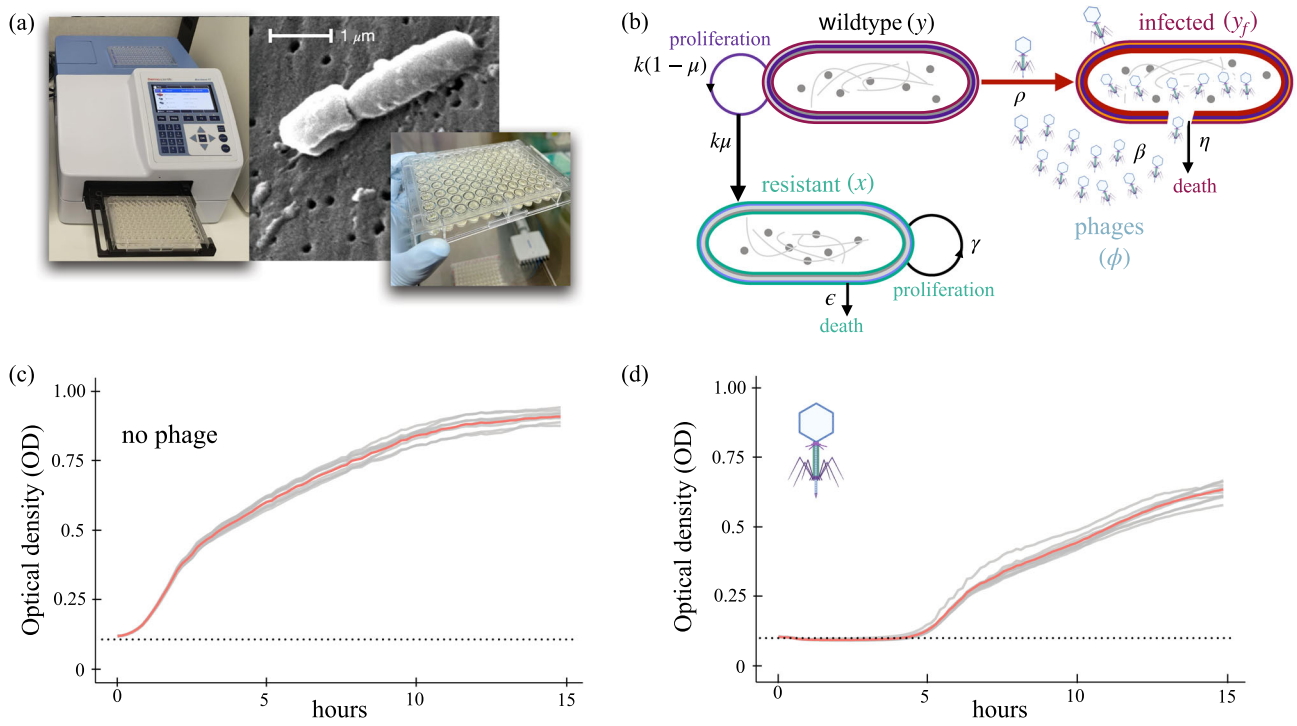

Fig. 2 Experimental system and modeled interactions. a Experimental setup to track the population dynamics of *Klebsiella pneumoniae* (strain Kpn63). The electron microscope image shows two bacteria cells (image by Janice Carr/CDC–CDC, Atlanta (USA) from Wikipedia). **b** Processes modeled in this work. We consider a wild-type (wt) population of bacteria (y) that can become infected (y_f) by phages (ϕ). The wt strains can mutate during replication and generate phage-resistant cells (x). The stoichiometry of the whole interactions is provided in reactions (1)-(7), modeled with Eqs. (8)-(11). **c** Growth curves for *Klebsiella pneumoniae* (strain Kpn63) without phages measured with the optical density (OD). We show eight replicates with an initial condition of bacteria with OD = 0.1. **d** Kpn63 dynamics with an initial population also with OD = 0.1 in the presence of phages. The horizontal dotted lines show the limit detection of the OD measures

ents; accordingly, this population is excluded from the logistic growth term. Although the proliferation rate of phage-resistant bacteria is allowed to differ from that of the wild-type strain, experimental measurements indicate that this difference is small [37]. Once a wild-type cell is infected, it is assumed to be refractory to further infection. All model parameters, together with their biological interpretation, numerical values, and units, are summarized in Table 1 (see also Fig. 1).

4 Results and discussion

In this section, we first compute the equilibria of the system (8)-(11). Second, we study their stability and bifurcations. Finally, we provide a sensitivity analysis of the system response upon changes in parameters and initial conditions by exploring the variational equations.

4.1 Equilibria and stability analysis

The equilibrium points of the system (8)-(11) are those points $(y^*, y_f^*, x^*, \phi^*)$ satisfying

$$k\,(1-\mu)\,y^*\,w(y^*,x^*) - \rho\,y^*\,\phi^* = 0, \tag{13}$$

$$\rho\,y^*\,\phi^* - \eta\,y_f^* = 0, \tag{14}$$

$$(k\,\mu\,y^* + \gamma\,x^*)\,w(y^*,x^*) - \varepsilon\,x^* = 0, \tag{15}$$

$$\beta\,\eta\,y_f^* - \rho\,y^*\,\phi^* = 0. \tag{16}$$

We calculate the solutions of this system, distinguishing two cases: (I) $y^* \neq 0$ and (II) $y^* = 0$.

Case I: $y^* \neq 0$. From the condition (14), it follows that $\eta\,y_f^* = \rho\,y^*\,\phi^*$. Substituting in (16), we obtain $(\beta - 1)\,\rho\,y^*\,\phi^* = 0$. Since $\beta > 1$ and $\rho > 0$, we conclude that $\phi^* = 0$ and, therefore, $\eta\,y_f^* = 0$. Since $\eta > 0$, we also obtain $y_f^* = 0$. Under these conditions, the equation (13) reduces to $w(y^*, x^*) = 0$. Then, $y^* = C - x^*$. Substituting in (15), it follows that $x^* = 0$ because $\varepsilon > 0$. Hence, we obtain an equilibrium point at $(C, 0, 0, 0)$, which we denote hereafter by P_1. This equilibrium point involves the persistence of only the *Klebsiella pneumoniae* wt strain achieving the maximum population (i.e., the carrying capacity C).

Table 1 Parameters of Eqs. (8)-(11). We display the symbols, the biological meaning, the values, and the units of each parameter. The values are set following the experimental results in Ref. [37]. In all these experiments $\varepsilon < \gamma$ and $\beta \gg 1$, so we assume the lower bound $\beta > 1$ to hold, since infected bacteria produce large amounts of phages [37]. Here CFU stands for colony-forming units and PFU for plaque-forming units. The time unit used throughout this work is $[t] = hours$

Parameter	Biological meaning	Range	Units
k	Intrinsic growth rate of susceptible wild-type bacteria	$0 < k < 1$	t^{-1}
γ	Replication rate of phage-resistant bacteria	$0 < \gamma < 1$	t^{-1}
μ	Fraction of resistant bacteria generated from susceptible ones	$0 < \mu < 1$	Dimensionless
ρ	Infection rate of susceptible bacteria by phages	$0 < \rho < 1$	$\text{mL} \cdot \text{PFU}^{-1} \cdot t^{-1}$
η	Death rate of infected bacteria due to phages	$0 < \eta < 1$	t^{-1}
β	Burst size (number of phages released upon bacterial lysis)	$\beta > 1$	$\text{PFU} \cdot \text{CFU}^{-1} \cdot t^{-1}$
ε	Decay rate of phage-resistant bacteria	$0 < \varepsilon < 1$	t^{-1}

Case II: $y^* = 0$. First, note that the condition (13) is trivial in this case. From the condition (14), it follows that $y_f^* = 0$. Under these conditions, the equation (16) is satisfied, and (15) is equivalent to the equation

$$\gamma\, x^* \left(1 - \frac{x^*}{C}\right) - \varepsilon\, x^* = 0,$$

for any value of ϕ^*. Therefore, we obtain two lines of equilibria, determined by the two solutions of the above expression, $x^* = 0$ and $x^* = C(1 - \varepsilon/\gamma)$. In what follows, we denote these two straight lines of equilibria by

$$R_0 \equiv \{(0, 0, 0, \theta^+) : \theta^+ \in \mathbb{R}^+\},$$
$$R_+ \equiv \{(0, 0, C(1 - \varepsilon/\gamma), \theta^+) : \theta^+ \in \mathbb{R}^+\}.$$

Remark 1 We take only the biologically meaningful part of the straight lines, $\theta^+ \geq 0$. In addition, we also require the condition $C(1 - \varepsilon/\gamma) > 0$ to be satisfied, i.e., $\varepsilon < \gamma$, in agreement with the experiments performed in Ref. [37].

Before presenting the formal stability results, it is useful to outline the structure of the phase space at a conceptual level. The system admits equilibria corresponding to wild-type dominance, phage extinction, and resistant–phage coexistence. Remarkably, the latter does not occur at an isolated point but along a continuum of states parameterized by phage density. As shown below, the stability properties transverse to this continuum determine whether the system converges to coexistence or clearance. The following result follows.

Theorem 1 *System* (8)-(11)*, with parameter values restricted to those given in Table 1, has an unstable hyperbolic equilibrium point at* $P_1 = (C, 0, 0, 0)$*, which is of saddle type* $(dim(W^s(P_1)) = 3$ *and* $dim(W^u(P_1)) = 1)$*. Moreover, under the condition* $\varepsilon < \gamma$*, the system has two non-negative half-lines of equilibria, which satisfy*

i) $R_0 = \{(0, 0, 0, \theta^+) : \theta^+ \in \mathbb{R}^+\}$ *is unstable,*

ii) $R_+ = \{(0, 0, C(1 - \varepsilon/\gamma), \theta^+) : \theta^+ \in \mathbb{R}^+\}$ *is unstable for* $\theta^+ < \theta_+^*$ *and locally stable for* $\theta^+ > \theta_+^*$*, where* $\theta_+^* \equiv \frac{1}{\rho\gamma} k(1 - \mu)\varepsilon$.

Proof The Jacobian matrix of the system (8)-(11) is given by

$$J_F(y, y_f, x, \phi) = \begin{pmatrix} k(1-\mu)\left(w(y,x) - \frac{y}{C}\right) - \rho\,\phi & 0 & -\frac{k(1-\mu)\,y}{C} & -\rho\, y \\ \rho\,\phi & -\eta & 0 & \rho\, y \\ k\,\mu\left(w(y,x) - \frac{y}{C}\right) - \frac{\gamma\, x}{C} & 0 & \gamma\left(w(y,x) - \frac{x}{C}\right) - \varepsilon - \frac{k\,\mu\, y}{C} & 0 \\ -\rho\,\phi & \beta\,\eta & 0 & -\rho \end{pmatrix}.$$

The characteristic polynomial associated with the Jacobian matrix at the equilibrium point P_1 is

$$p(\lambda) = c_0 + c_1\lambda + c_2\lambda^2 + c_3\lambda^3 + \lambda^4$$

with

$$c_0 = C\rho\eta k\varepsilon(1 - \beta)(1 - \mu),$$
$$c_1 = k\varepsilon(\eta + C\rho)(1 - \mu) + C\rho\eta(\varepsilon + k)(1 - \beta),$$
$$c_2 = C\rho\eta(1 - \beta) + k\varepsilon(1 - \mu) + (\eta + C\rho)(\varepsilon + k),$$
$$c_3 = \varepsilon + k + \eta + C\rho.$$

By carefully manipulating the above polynomial expression, we write p as the product of the following two quadratic polynomials

$$q_1(\lambda) = \lambda^2 + (\eta + C\rho)\lambda + C\rho\eta(1 - \beta),$$
$$q_2(\lambda) = \lambda^2 + (\varepsilon + k)\lambda + k\varepsilon(1 - \mu).$$

Therefore, the eigenvalues related to the equilibrium point P_1 are easily computed as the roots of q_1 and q_2. First, we compute the roots of q_1,

$$\lambda_{1,2} = \frac{-(\eta + C\rho) \pm \sqrt{(\eta + C\rho)^2 - 4C\eta\rho\,(1 - \beta)}}{2}.$$

Since the parameters of our model take positive values and $\beta > 1$, the discriminant is always positive, $\Delta = (\eta + C\rho)^2 +$

$4C\eta\rho\,(\beta-1) > 0$. Moreover, as $4C\eta\rho\,(\beta-1) > 0$, it follows that $\eta + C\rho < \sqrt{\Delta}$. Hence, these eigenvalues are real and of opposite sign, $\lambda_1 > 0$ and $\lambda_2 < 0$. Second, the roots of q_2 are

$$\lambda_{3,4} = \frac{-\varepsilon - k \pm \sqrt{(\varepsilon - k)^2 + 4k\varepsilon\mu}}{2}.$$

We obtain that both eigenvalues are real, since $(\varepsilon - k)^2 + 4k\varepsilon\mu > 0$. Regarding the sign of the roots, it is clear that $\lambda_4 < 0$. As for the sign of λ_3, since $4k\varepsilon(1-\mu) > 0$, it follows that

$$(\varepsilon + k)^2 > (\varepsilon + k)^2 - 4k\varepsilon(1-\mu)$$

and

$$-(\varepsilon + k) + \sqrt{(\varepsilon + k)^2 - 4k\varepsilon(1-\mu)} < 0.$$

Therefore, this eigenvalue is negative ($\lambda_3 < 0$). In summary, P_1 is an unstable hyperbolic equilibrium point of saddle type, with $\dim(W^s(P_1)) = 3$ and $\dim(W^u(P_1)) = 1$.

i) The Jacobian matrix associated with the line of equilibria $R_0 = \{(0,0,0,\theta^+) : \theta^+ \geq 0\}$ is given by the block-lower-triangular matrix

$$J_F^0 = \left(\begin{array}{cc|cc} k(1-\mu) - \rho\theta^+ & 0 & 0 & 0 \\ \rho\theta^+ & -\eta & 0 & 0 \\ \hline k\mu & 0 & \gamma - \varepsilon & 0 \\ -\rho\theta^+ & \beta\eta & 0 & 0 \end{array}\right),$$

whose spectrum is directly computed:

$$\mathrm{spec}(J_F^0) = \left\{k(1-\mu) - \rho\theta^+ : \theta^+ \geq 0\right\} \cup \{-\eta, \gamma - \varepsilon, 0\}.$$

As $\gamma > \varepsilon$, all equilibrium points on R_0 have an unstable direction (associated with the positive eigenvalue $\gamma - \varepsilon$). Therefore, the line of equilibrium points R_0 is unstable.

ii) The Jacobian matrix J_F evaluated at points on the half-line $R_+ = \{(0,0,C(1-\varepsilon/\gamma),\theta^+) : \theta^+ \in \mathbb{R}^+\}$ is given by the block-lower-triangular matrix

$$J_F^+ = \left(\begin{array}{cc|cc} k(1-\mu)\frac{\varepsilon}{\gamma} - \rho\theta^+ & 0 & 0 & 0 \\ \rho\theta^+ & -\eta & 0 & 0 \\ \hline k\mu\frac{\varepsilon}{\gamma} + \varepsilon - \gamma & 0 & \varepsilon - \gamma & 0 \\ -\rho\theta^+ & \beta\eta & 0 & 0 \end{array}\right).$$

We easily obtain

$$\mathrm{spec}(J_F^+) = \left\{k(1-\mu)\frac{\varepsilon}{\gamma} - \rho\theta^+ : \theta^+ \geq 0\right\} \cup \{-\eta, \varepsilon - \gamma, 0\}.$$

Depending on the values of θ^+, we distinguish two cases. On the one hand, there exists an unstable direction when $k(1-\mu)\frac{\varepsilon}{\gamma} > \rho\theta^+$. By defining $\theta_+^* \equiv \frac{1}{\rho\gamma}k(1-\mu)\varepsilon$, we obtain the line

$$r_1^+ \equiv \{(0,0,C(1-\varepsilon/\gamma),\theta^+) : 0 \leq \theta^+ < \theta_+^*\},$$

which consists of unstable equilibrium points. On the other hand, we get the line

$$r_2^+ \equiv \{(0,0,C(1-\varepsilon/\gamma),\theta^+) : \theta^+ > \theta_+^*\},$$

consisting of equilibrium points with three stable directions and one central direction.

We refer the reader to the works by Fiedler and Liebscher on stability of lines of equilibria [38, 39].

Remark 2 The ϕ-direction related to the zero eigenvalue, which appears respectively in the spectrum of J_F^0 and J_F^+, is entirely linked to the existence of the half-lines of equilibrium points. Each half-line, R_0 and R_+, acts as a degenerate normally hyperbolic invariant manifold. Therefore, its dynamics are governed by the transversal hyperbolic directions. In particular, as the threshold value θ_+^* is crossed along R_+, a change in the stability of the equilibria occurs. This indicates that the limiting (stable) phage population must be sufficiently large to ensure that all susceptible bacteria become infected, leaving only a residual population of resistant bacteria. Consequently, smaller initial phage populations are favoured to initially grow more rapidly before stabilizing near their limiting value. The convergence of trajectories to a stable equilibrium in R_+ will be addressed later.

For completeness, we verify the nonnegativity and convergence of the solutions for biologically meaningful initial conditions, i.e., nonnegative initial data with x and y bounded by the carrying capacity, as expected biologically.

Definition 1 We say that $(y(0), y_f(0), x(0), \phi(0))$ are *biologically meaningful* if

$$(y(0), y_f(0), x(0), \phi(0)) \in \Omega \text{where}$$
$$\Omega := \left\{(y, y_f, x, \phi) \in \mathbb{R}_+^4 : \; x + y \leq C\right\}.$$

We restrict the system to the biologically meaningful domain Ω, which is positively invariant.

Proposition 1 *Solutions of the system (8)–(11), with parameter values given in Table 1 and biologically meaningful initial conditions (Definition 1), exist for all $t \geq 0$ and satisfy*

$$(y(t), y_f(t), x(t), \phi(t)) \in \Omega \qquad \forall\, t \geq 0.$$

In addition, for all $t \geq 0$

i) $0 \le y_f(t) \le N$, *where* $N = \max\{y(0) + y_f(0),\ C + k(1-\mu)C/\eta\}$,
ii) $0 \le \phi(t) \le M$, *where* $M = \max\{\beta(y(0) + y_f(0)) + \phi(0),\ \beta(C+N) + k(1-\mu)\beta/\rho\}$.

Proof We begin by proving that Ω is positively invariant. Since the solutions are continuous, any component can only become negative by crossing zero. To verify whether this is possible, we check the vector field on each coordinate hyperplane:

- If $y = 0$, equation (8) implies that $\dot{y} = 0$, and thus y cannot cross into $y < 0$.
- When $y_f = 0$, equation (9) yields $\dot{y_f} = \rho y\phi \ge 0$ in $\mathbb{R}^4_+$.
- For $x = 0$, equation (10) shows that $\dot{x} = k\mu y\omega(y, 0) \ge 0$ whenever $0 \le y \le C$ (because then $\omega(y, 0) = 1 - y/C \ge 0$).
- If $\phi = 0$, then (11) implies $\dot{\phi} = \beta\eta y_f \ge 0$ in $\mathbb{R}^4_+$.

Hence, nonnegative initial data remain nonnegative whenever $y \le C$, i.e., $\mathbb{R}^4_+$ is forward invariant. To prove that the region $x + y \le C$ is forward invariant (which is stronger than $y \le C$), we consider x and y on the boundary $x + y = C$. Since $\omega(y, x) = 0$, it follows from (8) and (10) that $\dot{x} = -\varepsilon x \le 0$ and $\dot{y} = -\rho y\phi \le 0$ in $\mathbb{R}^4_+$. Therefore, Ω is positively invariant. In particular, $0 \cdot x(t) + y(t) \cdot C$ for all $t \ge 0$, which shows that they are bounded above by C.

In order to analyze the boundedness of y_f, we set $r(t) := y(t) + y_f(t)$. Using (8)–(9),

$$\begin{aligned}\dot{r}(t) &= \dot{y}(t) + \dot{y_f}(t) = k(1-\mu)\, y\, \omega(y, x) - \eta y_f \\ &\le k(1-\mu)\, y - \eta y_f = k(1-\mu)\, y - \eta(r - y).\end{aligned}$$

Since $0 \le y(t) \le C$ for all $t \ge 0$, we obtain the inequality

$$\dot{r}(t) \le (k(1-\mu) + \eta)\, C - \eta\, r(t).$$

By comparison, we have $r(t) \le \max\{r(0),\ C + k(1-\mu)C/\eta\}$. As $0 \le y_f(t) \le r(t)$, claim *i)* follows.

Finally, we establish the boundedness of $\phi(t)$ by defining

$$q(t) := \beta\big(y(t) + y_f(t)\big) + \phi(t).$$

Using (8)–(11), we compute

$$\begin{aligned}\dot{q}(t) &= \beta k(1-\mu)\, y\, \omega(y, x) - \rho y\phi \le \beta k(1-\mu)\, y \\ &\quad - \rho y\phi = y\big(\beta k(1-\mu) - \rho\phi\big).\end{aligned}$$

By the comparison principle, $q(t) \le \max\{q(0),\ \beta(C + N) + \beta k(1-\mu)/\rho\}$. Since $\phi(t)$ satisfies $0 \le \phi(t) \le q(t)$, claim *ii)* follows.

The result below guaranties that all nonnegative solutions with biologically meaningful initial conditions approach an equilibrium.

Proposition 2 *Solutions to the system* (8)–(11)*, with parameter values given in Table 1 and any initial condition* $(y(0), y_f(0), x(0), \phi(0)) \in \Omega$*, converge to a nonnegative equilibrium.*

Proof Consider the function

$$L(y, y_f, x, \phi) := -\big((\beta - 1)y + \beta y_f + \phi\big),$$

defined in a compact positive invariant set $\Omega^c \subset \Omega$.[1] Using (8)–(11), we compute

$$\begin{aligned}\dot{L} &= -(\beta - 1)\dot{y} - \beta\dot{y_f} - \dot{\phi} \\ &= -(\beta - 1)k(1-\mu)\, y\, \omega(y, x) \le 0 \quad \forall t \ge 0,\end{aligned}$$

since Ω is forward invariant and $\omega(y, x) \ge 0$ for all $t \ge 0$.

Thus $L(t)$ is nonincreasing along trajectories. As all components are bounded, L is bounded from below, and hence there exists $\ell \in \mathbb{R}$ such that $L(t) \to \ell$ as $t \to \infty$.

By LaSalle's invariance principle [23], the ω-limit set of any trajectory is contained in the largest invariant subset of

$$\begin{aligned}&\{(y, y_f, x, \phi) \in \Omega^c \mid \dot{L}(y, y_f, x, \phi) = 0\} \\ &= \Omega^c|_{\{y=0\}} \cup \Omega^c|_{\{x+y=C\}}.\end{aligned}$$

The largest invariant subset of this set is precisely the equilibrium set[2]

$$\mathcal{E} := (P_1 \cup R_0 \cup R_+) \cap \Omega^c,$$

where we only consider R_+ when $\gamma > \varepsilon$ (so that it is included in Ω^c). Hence, $\omega(z_0) \subset \mathcal{E}$, where $z_0 := (y(0), y_f(0), x(0), \phi(0)) \in \Omega$. Moreover, since $L(t) \to \ell$ as $t \to \infty$, every point $p \in \omega(z_0)$ must satisfy $L(p) = \ell$. Therefore,

$$\omega(z_0) \subset \mathcal{E} \cap \{L = \ell\}.$$

Now, along the equilibrium branches, we have

$$\begin{aligned}&L(C, 0, 0, 0) = -(\beta - 1)C, \qquad L(0, 0, 0, \phi^*) = -\phi^*, \\ &\quad L\big(0, 0, C(1 - \varepsilon/\gamma), \phi^*\big) = -\phi^*.\end{aligned}$$

Therefore, on each connected component of $\mathcal{E}$, the level set $\{L = \ell\}$ contains at most one point.

[1] As our populations are bounded, we can always extract a compact positive invariant subset of Ω for each initial condition.

[2] Note that the intersection with Ω^c would only affect R_0 and R_+ by limiting the value of ϕ to its bound.

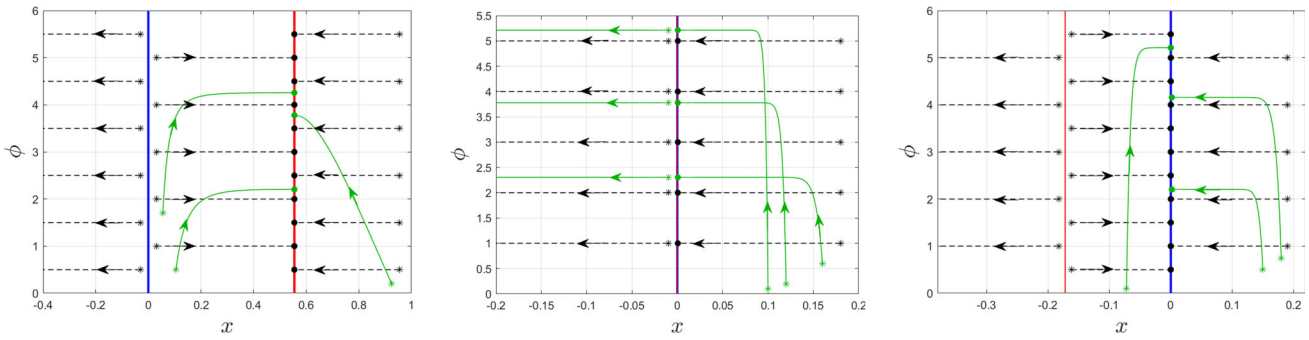

Fig. 3 Phase portraits and bifurcations. Orbits of the system (8)–(11) projected on the invariant plane $\Pi = \{y = 0, y_f = 0\}$ for different values of ε. The other parameters are fixed, as indicated in the table of Fig. 1 (estimated with the Bayesian inference (BI)). The half-lines of equilibrium points R_+ and R_0 are displayed in red and blue, respectively. Initial conditions are marked with asterisks, and the end of orbits with dots. Orbits with initial conditions on the plane Π are shown in black dashed lines, while those with initial conditions $y = 0$ and $y_f \neq 0$ (projected onto the invariant plane) are shown in green lines. (Left) $\varepsilon < \gamma$ with $\varepsilon = 0.1904$: The line R_+ is an attractor, and the line R_0 is repulsive. (Middle) $\varepsilon = \gamma$ with $\varepsilon = 0.5794$: Both half-lines coincide (purple), forming a single line of half-stable equilibrium points. (Right) $\varepsilon > \gamma$ with $\varepsilon = 0.7$: The line R_+ becomes unstable and negative on the x-axis, losing biological meaning, while the line R_0 becomes stable. Orbits shown for negative values of x correspond to cases with no biological meaning

Finally, since the ω-limit set of a bounded trajectory is compact, invariant, and connected, it follows that $\omega(z_0)$ consists of a single point. Therefore, the trajectory converges to one equilibrium of the system. Moreover, for all initial conditions not lying on the stable manifolds of P_1 or of the equilibria on R_0 and r_1^+, trajectories converge to one of the stable equilibrium points in R_+ (i.e. r_2^+).

To conclude the analysis carried out in this section, we consider the dynamics of the system by using the values of the parameters estimated with the Bayesian inference (BI) in the experiments [37] (see Fig. 1). We notice that using the values obtained with the Levenberg-Marquardt (LM) method would result in the same qualitative dynamics. The equilibrium points using these estimated values are given by

$$P_1 = (0.8270, 0, 0, 0), \quad R_0 = \{(0, 0, 0, \theta^+) : \theta^+ \geq 0\},$$
$$R_+ = \{(0, 0, 0.5552, \theta^+) : \theta^+ \geq 0\},$$

and the spectra of their associated Jacobian matrices are

$$\begin{aligned}
\text{spec}(J_F^1) &= \{9.7493, -11.3685, -0.0897, -0.6663\},\\
\text{spec}(J_F^0) &= \{0.3140 - 0.9359\,\theta^+ : \theta^+ \geq 0\}\\
&\quad \cup \{-0.8452, 0.3890, 0\},\\
\text{spec}(J_F^+) &= \{0.1032 - 0.9359\,\theta^+ : \theta^+ \geq 0\}\\
&\quad \cup \{-0.8452, -0.3890, 0\}.
\end{aligned}$$

Following the results above, considering the estimated parameter values from the data, the orbits will move towards the half-line R_+, since the other equilibria, the point P_1 and the half-line R_0, are unstable. Due to the transverse stability of r_2^+, the only asymptotic state the system can achieve is the stable part of the half-line R_+. The point separating the stable and unstable regions along the line R_+ is given by $\theta_+^* = 0.1103$, with $x^* = 0.5552$. This prediction is in agreement with the values obtained for the phage-resistant mutants in the experiments. The fits performed with both the LM and the BI showed a population of phage-resistant cells rapidly out-competing the susceptible ones together with the extinction of the infected bacteria. The dynamics for the phage-resistant cells started saturating at approximately 15-16 h, achieving a population value of $x(t = 16) \approx 0.56$ (see Fig. 1).

4.2 Bifurcations

The computation of the equilibria of Eqs. (8)-(11) and the analysis of their linear stability allow us to identify the parameters that cause qualitative changes in the dynamics. That is, the identification of bifurcations. Most of these bifurcations, with one exception, are not biologically relevant, as they occur for parameter values outside the biologically admissible range.

Among all the assumptions made regarding the model parameters (see Table 1), there is only one that can be modified in our model without entirely losing biological meaning: $\gamma > \varepsilon$. Although such a bifurcation will never occur in the case of the bacteria strain studied here, that is, under the estimated parameter values, both the parameters γ and ε could vary for other bacterial strains. Slowing the growth of multidrug-resistant (MDR) bacteria that have also developed

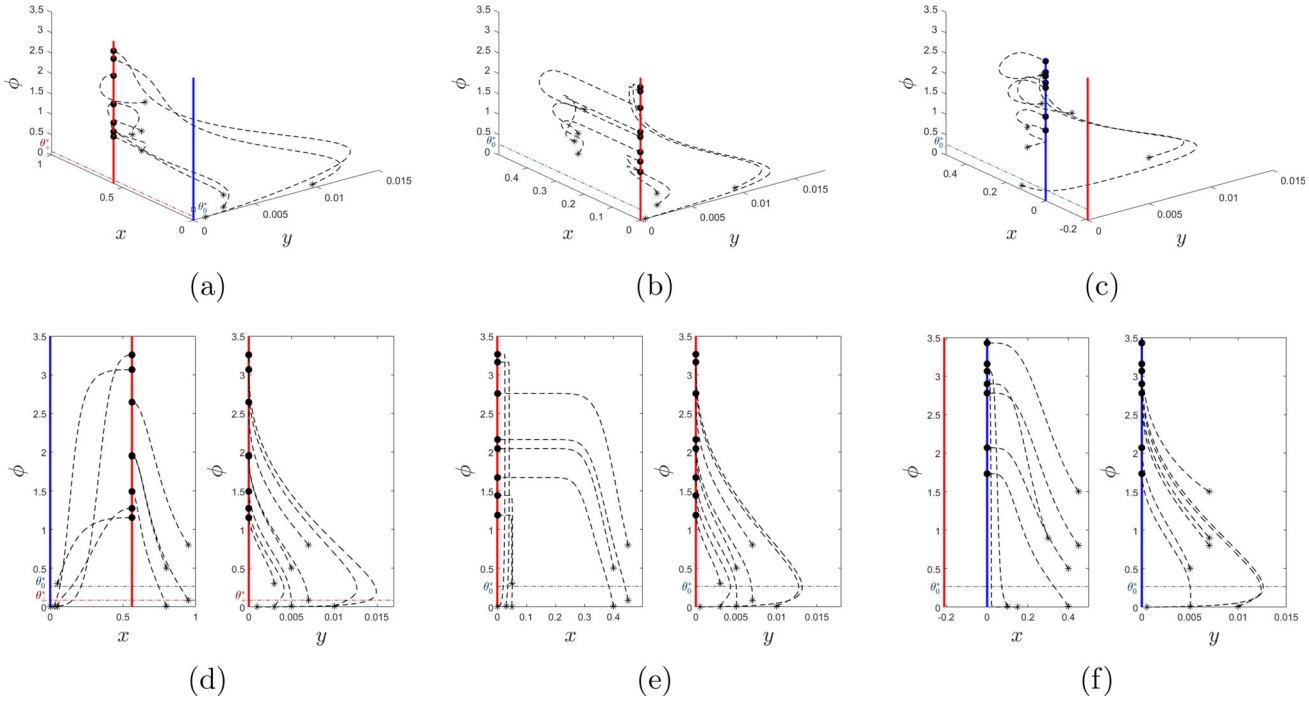

Fig. 4 Orbits of the system (8)–(9) around the bifurcation associated with the parameter ε. The line R_+ is shown in red and the line R_0 in blue. The start of each orbit is indicated by an asterisk and the end by a dot. For all simulations, parameter values are taken from the table in Fig. 1, except for the bifurcation parameter ε, which is varied. (**a**)–(**c**) Orbits of the populations x, y, and ϕ for different initial conditions outside the invariant plane $\{y = 0, y_f = 0\}$. (**a**) Example with $\varepsilon = 0.1904 < \gamma$. The line R_+ is attractive, while the line R_0 is repulsive. (**b**) The case $\varepsilon = \gamma = 0.5794$ makes both lines coincide, forming a single equilibrium line R_0 containing half-stable equilibria. (**c**) Here $\varepsilon = 0.7 > \gamma$ is selected. The line R_+ becomes unstable and loses biological relevance, while the line R_0 becomes stable. (**d**)–(**f**) Projections of the orbits from panels (**a**)–(**c**), respectively, onto the (x, ϕ) and (y, ϕ) planes. We only show nonnegative orbit values with biological meaning

resistance to bacteriophages is highly challenging and likely requires multifaceted strategies. One approach could involve phage cocktails or engineered phages, which target multiple bacterial receptors or deliver lethal genetic payloads [21]. CRISPR-Cas systems, delivered via phages or conjugative plasmids, can precisely eliminate resistant strains by targeting essential or resistance genes [8]. Bacteria often pay a fitness cost for resistance, which could be exploited by adjusting environmental conditions (e.g., nutrient limitation) or by introducing competitive strains weakening the growth of the phage-resistant strains. Quorum sensing inhibitors can also disarm bacteria without selecting for further resistance [33]. Moreover, phage-resistant bacteria could slow down growth or increase mortality if an antibiotic acting synergistically with bacteriophages is introduced. In this sense, phage-antibiotic therapies have shown promise in resensitizing bacteria to treatments [9].

In what follows, we analyze the bifurcation associated with the extinction of phage-resistant bacteria. All parameters are fixed at the values estimated using the Bayesian inference method (Fig. 1), with the exception of ε, which is treated as the bifurcation parameter. From a biological and therapeutic standpoint, bifurcations in this system correspond to qualitative shifts in treatment outcomes. Among all parameters, the effective mortality rate of phage-resistant bacteria (ε) plays a distinctive role, as it could be experimentally modulated through antibiotic exposure, immune-mediated clearance, or engineered phage strategies. We therefore examine ε as a control parameter governing transitions between resistant persistence and clearance.

First, we note that the spectrum of the Jacobian matrix at P_1 varies with ε, yet the instability of P_1 remains unaffected by the condition $\gamma > \varepsilon$. Accordingly, we focus solely on the changes along the half-lines of equilibria R_0 and R_+ as the bifurcation parameter varies. It is clear that the condition $\varepsilon = \gamma$ marks a change in the stability of the equilibrium lines in the x-direction, as suggested by the spectrum of the Jacobian associated with both lines. To explore this stability change in more depth, we restrict our analysis to the invariant plane $\Pi = \{y = 0, y_f = 0\}$. Since $\dot{y} = 0$ and $\dot{y}_f = 0$ under this restriction, the 4-dimensional system (8)-(11) is reduced to a 2-dimensional model. Moreover, on the invariant plane Π, we also obtain that $\dot{\phi} = 0$ for all values of ϕ. Thus, within this invariant plane, the variable ϕ remains constant and can

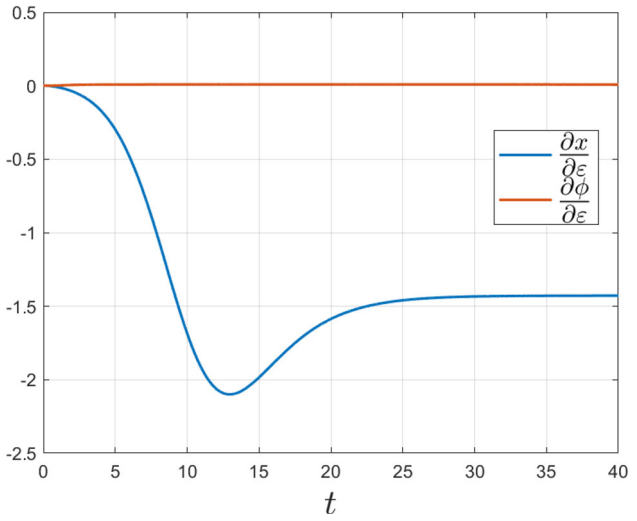

Fig. 5 Sensitivity analysis of x and ϕ as functions of ε over the time interval $t \in [0, 40]$, for the system given by equations (8)-(11). The estimated parameter values given in the table in Fig. 1 are used. Additionally, an initial condition very similar to that of the experiments [37] is taken, particularly, $(y_0, y_{f_0}, x_0, \phi_0) = (0.1, 0, 0, 1)$. The variable x shows a variation that increases slightly at the beginning but quickly stabilizes. The variable ϕ barely shows any variation. Only x and ϕ are shown in the figure, as y and y_f are negligible

be treated as a parameter in the reduced system. This means that the dynamics are effectively governed by the differential equation:

$$\dot{x} = x\left(\gamma - \varepsilon - \frac{\gamma}{C}x\right). \tag{17}$$

After the change of variable $z = \frac{\gamma}{C}x$, Eq. (17) can be written in the normal form of the transcritical bifurcation, i.e., $\dot{z} = \alpha z - z^2$ with $\alpha = \gamma - \varepsilon$. Figure 3 illustrates the dynamics of x and ϕ on the plane Π, by means of phase portraits for various values of the bifurcation parameter.

Although the transcritical bifurcation in the x-direction is fully characterized, it is important to clarify what occurs in the other two directions that were not considered. In fact, the eigenvalue in the y_f-direction, as verified in the previous section, is always negative ($-\eta < 0$). Therefore, the only direction that may cause instabilities is the y-direction. We describe the three cases to determine whether the dynamics of the equilibrium points along the half-lines indeed change.

As shown in the different panels of Fig. 4, for initial conditions with ϕ below a certain threshold, the orbits move away from the equilibrium points. However, once the orbit crosses this threshold (denoted θ_+^* in the case $\varepsilon < \gamma$ and θ_0^* in the other cases), attraction toward the corresponding equilibrium line begins. Furthermore, we observe that the higher the distance from the attracting equilibrium line, the faster the convergence; this is reflected in the eigenvalue in the y-direction becoming increasingly negative. Moreover, the local stability analysis of R_+, together with the behavior illustrated in Fig. 4, panels (d) and (f), allows us to propose a biologically significant interpretation of the observed phenomenon. For very small initial phage populations ϕ_0, the virus appears to develop a mechanism allowing it to persist, even when the bacterial population is significantly larger. Notably, there is an initial sharp decline in the resistant bacterial population, accompanied by a rapid growth of the phage population. From a biological perspective, if experimental validation confirms this mechanism, it could be exploited to induce a drastic initial reduction in resistant bacteria.

In summary, we have identified a global transcritical bifurcation in the x-direction involving the two half-lines of equilibria R_0 and R_+. We name it a global transcritical bifurcation because the collision and interchange of stability is not between two single points, but between a continuum of points at each line. Additionally, we have shown that, in the full system, the attracting half-line r_2^+ (present when $\varepsilon < \gamma$) loses stability in favor of r_2^0 as the bifurcation parameter ε crosses the critical threshold γ.

4.3 Sensitivity analysis

In this section, we provide a local sensitivity analysis of the model, exploring how changes in parameters and initial conditions impact the dynamics. Our approach follows the study of the variational equations outlined in Ref. [32]. Variational sensitivity analysis computes sensitivities by solving additional differential equations, providing accurate, continuous results in a single simulation. In contrast, standard methods (like finite differences, Monte Carlo sensitivity analysis, or variance-based methods) rely on repeated model evaluations with perturbed parameters, making them simpler but less efficient and more prone to numerical errors. Sensitivity analysis based on variational equations also provides key insights into the robustness of the mathematical model when subjected to uncertainties, whether in the model parameters or in the initial conditions. In the previous section, the parameter ε was identified as a key factor influencing the system's dynamics, acting as a bifurcation parameter. Given its importance, we begin the sensitivity study by examining the effects of small perturbations in ε. We then extend the same methodology to the remaining parameters of the model.

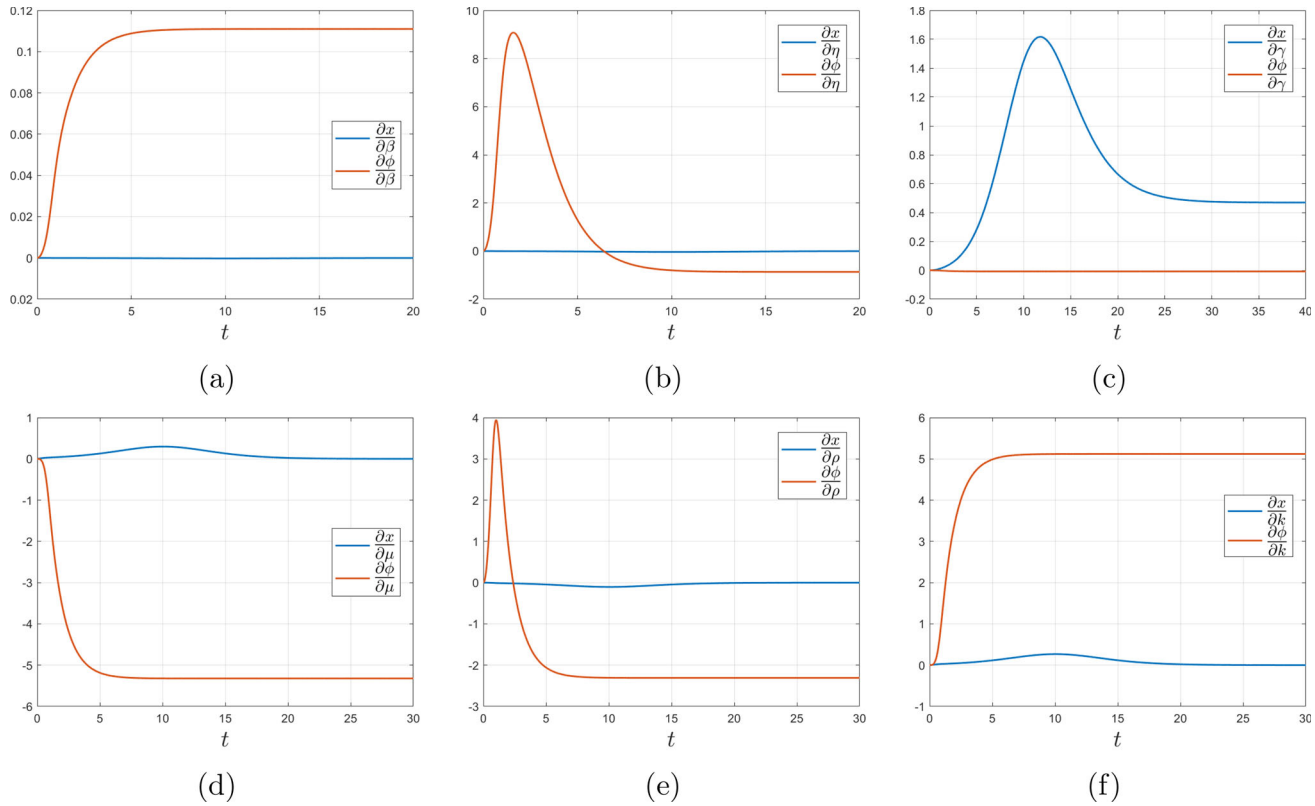

Fig. 6 Sensitivity analysis of x and ϕ as functions of the parameters of the system (8)-(11) for different time intervals. The estimated parameter values given in the table in Fig. 1 are used. Additionally, an initial condition very similar to that of the experiments [37] is taken, that is, $(y_0, y_{f\,0}, x_0, \phi_0) = (0.1, 0, 0, 1)$. (**a**) The variable ϕ shows a small variation with respect to parameter β, while x practically shows no variation. (**b**) The variable ϕ has a notable initial variation with respect to η, although it rapidly decreases. On the other hand, x shows no variation. (**c**) The variable ϕ barely fluctuates with respect to γ, while the variable x varies slightly at the beginning. (**d**) The variable ϕ varies rapidly initially with respect to μ, while the variable x barely moves. (**e**) The variable ϕ varies slightly with respect to ρ at the beginning and the variable x barely varies. (**f**) The variable ϕ shows some variation with respect to k, and the variable x shows hardly any changes

The sensitivity analyses for the parameters are studied from the following system of variational equations:

$$\begin{aligned}
\frac{d}{dt}\left(\frac{\partial y}{\partial \varepsilon}\right) &= \left[k(1-\mu)\left(1-\frac{x+2y}{C}\right)-\rho\phi\right]\frac{\partial y}{\partial \varepsilon} \\
&\quad -\frac{k(1-\mu)y}{C}\frac{\partial x}{\partial \varepsilon}-\rho y\frac{\partial \phi}{\partial \varepsilon}, \\
\frac{d}{dt}\left(\frac{\partial y_f}{\partial \varepsilon}\right) &= \rho\phi\frac{\partial y}{\partial \varepsilon}-\eta\frac{\partial y_f}{\partial \varepsilon}+\rho y\frac{\partial \phi}{\partial \varepsilon}, \\
\frac{d}{dt}\left(\frac{\partial x}{\partial \varepsilon}\right) &= \left[k\mu\left(1-\frac{x+2y}{C}\right)-\frac{\gamma x}{C}\right]\frac{\partial y}{\partial \varepsilon} \\
&\quad +\left[\gamma\left(1-\frac{2x+y}{C}\right)-\frac{k\mu y}{C}-\varepsilon\right]\frac{\partial x}{\partial \varepsilon}-x, \\
\frac{d}{dt}\left(\frac{\partial \phi}{\partial \varepsilon}\right) &= -\rho\phi\frac{\partial y}{\partial \varepsilon}-\rho y\frac{\partial \phi}{\partial \varepsilon}+\beta\eta\frac{\partial y_f}{\partial \varepsilon}.
\end{aligned} \tag{18}$$

Since the original system and the perturbed one share the same initial conditions, the variational equations must reflect this fact as well. Thus, they satisfy the following initial conditions:

$$\frac{\partial y}{\partial \varepsilon}(0)=0, \quad \frac{\partial y_f}{\partial \varepsilon}(0)=0, \quad \frac{\partial x}{\partial \varepsilon}(0)=0, \quad \frac{\partial \phi}{\partial \varepsilon}(0)=0.$$

We can numerically estimate the solutions of the system (18). The results of the analysis for the parameter ε show that the variations for y, y_f, or x are very small, being significant only for ϕ, as illustrated in Fig. 5. Actually, a value of $\partial\phi/\partial\varepsilon$ of about ~ 10 is not a very significant variation considering the order of magnitude of the phage population. In principle, we only consider a fluctuation truly significant when the order of magnitude of the derivative is higher (order 2 or above),

Next, we repeat this analysis for any parameter $\lambda \in \{\beta, \eta, \gamma, \nu, \rho, k\}$ of the model. The results of the analysis show that, as in the case of the parameter ε, the variations for y or y_f are very small, being of interest only those for x and ϕ. We illustrate the results obtained in Fig. 6.

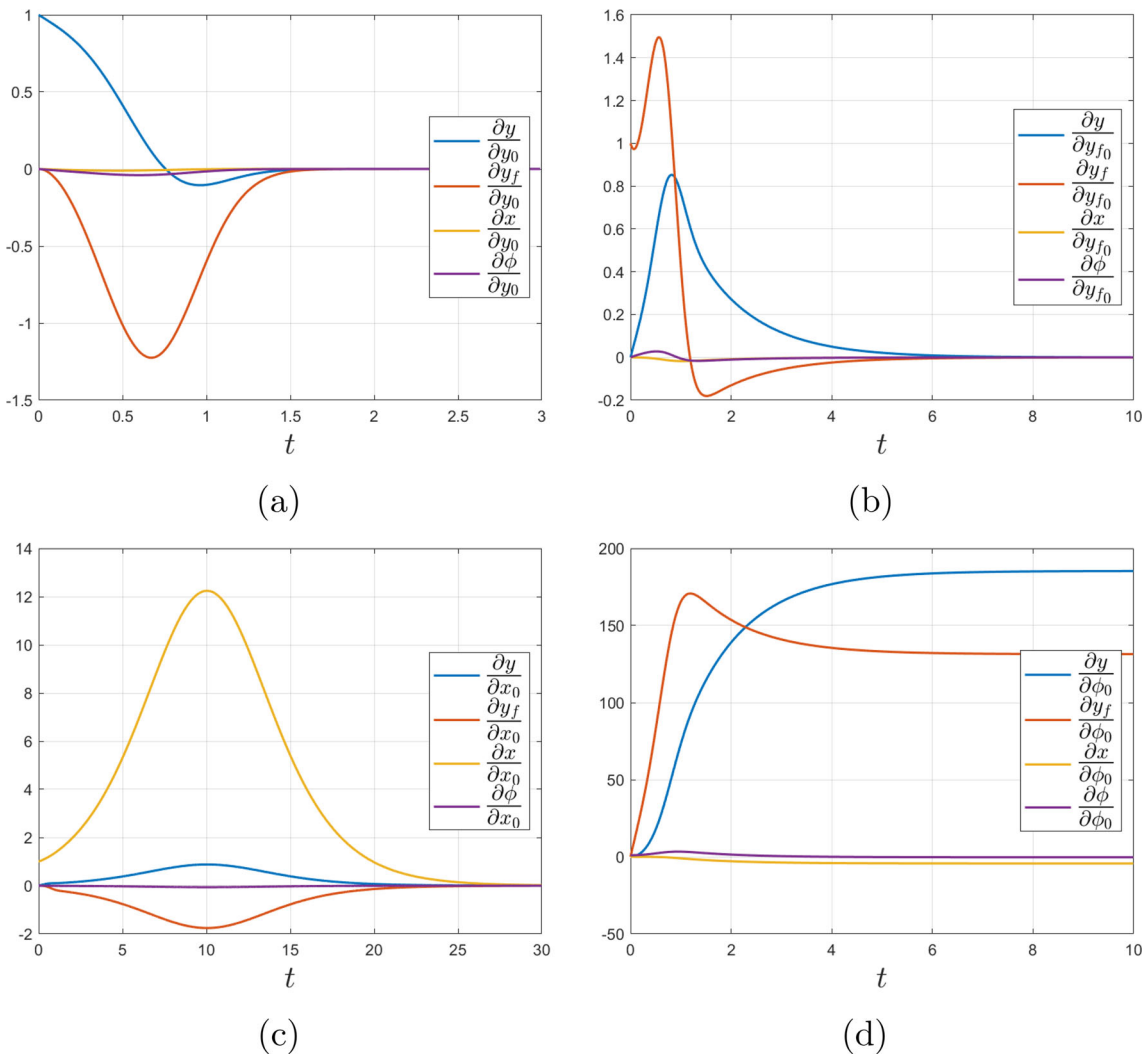

Fig. 7 Sensitivity analysis of y, y_f, x, and ϕ with respect to the initial conditions of the system (8)–(11) over different time intervals. The parameter values used correspond to those estimated in the table in Fig. 1. Additionally, the initial condition is chosen to closely resemble that of the experiments in Ref. [37], specifically $(y_0, y_{f_0}, x_0, \phi_0) = (0.1, 0, 0, 1)$. (**a**) The variables y and y_f exhibit a small initial variation with respect to the initial condition y_0 that rapidly decreases, while the variables x and ϕ show almost no change. (**b**) All variables except ϕ, which remains nearly constant, show an initial variation relative to the initial condition y_{f_0} that quickly diminishes. (**c**) The variables y and y_f display very limited variation with respect to the initial condition x_0. The population x exhibits the greatest sensitivity, although this also decreases over time, and the population ϕ again shows very little sensitivity. (**d**) The variables y and y_f show a notable variation with respect to the initial condition ϕ_0. The variables x and ϕ exhibit a small initial variation that eventually decreases

We conclude that the model (8)-(11) is quite robust in the sense that the results are not conditioned by perturbations in the parameters. However, we should note that in the particular case of the variable ϕ some sensitivity to the parameters can be appreciated, particularly to η, where the highest peak value of all is reached (see Fig. 6, panel (b)).

To complete the sensitivity analysis of the model, we study its behavior under variations in the initial conditions. Of particular interest is the sensitivity with respect to the initial phage concentration, ϕ_0. To achieve this, we apply a method based on parameter sensitivity analysis, also relying on the variational equations. We follow similar computations as in Ref. [32].

The results obtained for the initial conditions y_0 and y_{f_0} show that the variations in the different variables are very small [see Fig. 7(a,b)]. The perturbed solutions quickly stabilize, approaching the unperturbed solution. In the case of the initial condition x_0, we observe some variation, especially in the variable x. However, all variables eventually converge to the unperturbed solution [see Fig. 7(c)]. Finally, the initial condition ϕ_0 has the greatest impact on the system's sensitivity, as observed in our results. Much larger variations occur

than in the other cases, particularly for the populations y and y_f [see Fig. 7(a,b)]. This can also be interpreted as the model dynamics having a strong dependence on the initial condition ϕ_0. Except for this last case, no significant variation is observed for any of the populations in the other results; all obtained values remain within orders of magnitude that support the robustness of the model.

In general, the sensitivity analyses conducted for both parameters and initial conditions allow us to conclude that our model is very stable and robust. That is, small perturbations in the fixed conditions of the model–whether initial conditions or parameter values–do not produce significant fluctuations in the solutions.

Biologically, this robustness implies that the emergence of resistant-dominated outcomes is not an artifact of fine-tuned parameter choices or experimental noise. Instead, the qualitative behavior is structurally stable across broad parameter ranges, reinforcing the relevance of the identified quasineutral manifold for real phage–bacteria systems.

5 Conclusions

The global proliferation of multidrug-resistant (MDR) bacteria poses a critical threat to public health by compromising the efficacy of conventional antibiotic therapies and necessitating the development of alternative antimicrobial strategies [1]. With antibiotic development pipelines lagging behind clinical needs [17], phages are regaining attention as a viable therapeutic option [43]. Clinical cases and trials have demonstrated phage efficacy against antibiotic-resistant infections [42]-[19], and engineered phages and phage cocktails are being explored to broaden host range and mitigate resistance [4]. Therapies based on combining phages with antibiotics are an important topic of current research from both the experimental [24, 30, 31, 34] and theoretical [25, 40] approaches.

Implementing phage therapy effectively requires a deep understanding of phage-bacteria dynamics, particularly to address the problem of the emergence of phage-resistant strains. Mathematical modeling provides a powerful tool to simulate and predict these interactions, supporting optimized treatment strategies [27]. *In vitro* experiments, such as those recently reported by Rodríguez et al. [37], allow estimation of key parameters like infection rates, burst sizes, and the likelihood of the emergence of phage-resistant bacteria. In the experiments carried out in Ref. [37], the initial population of *Klebsiella pneumoniae* was depleted by the phages, but after a few hours, the population of bacteria started growing again due to the emergence or overgrowth of phage-resistant strains. Previous *in vitro* experiments [7, 12, 26, 28] and ecological models [3, 28, 44] of phage-bacteria systems predict broad regimes of coexistence among phage and bacteria populations. In many instances, co-culturing of phage and bacteria together leads to the emergence of persistent coevolution, maintaining their populations in the long term through the so-called Red Queen dynamics [2, 12, 22].

In this work, we have analyzed the model introduced in Ref. [37], which was calibrated with *in vitro* data on bacteria-phage dynamics. Here we have studied the equilibria and bifurcations that govern coexistence and clearance scenarios for the phage-resistant strain(s). We have identified coexistence of phage-resistant bacteria with phages by means of a degenerate normally hyperbolic invariant manifold (NHIM). This degenerate NHIM is indeed a line of quasi-neutral equilibria with an unstable and a stable part. This NHIM, in the the deterministic approach analyzed here, involves that different close initial conditions can be attracted toward different regions of the stable line, i.e., non-chaotic sensitivity to initial conditions. The presence of quasineutral manifolds has been described in other models in theoretical biology. For instance, lines or curves of equilibria have been identified in prey-predator models given by differential [14] and partial differential [16] equations, in Lotka-Volterra competition models [14, 29], in strains' competition models of disease dynamics [20], in models of RNA genome replication [41], and in host-parasite systems [18]. Other dynamical systems have been shown to be governed by higher-dimensional degenerate NHIMs involving planes filled with equilibria. These neutral surfaces have been characterized in predator–prey models with Holling type III functional responses [15] and in socio-economical models [5] and, more recently, in a mathematical model for betacoronavirus between-cell infections [32].

Summarizing, our work provides insights into simple phage-bacteria dynamics by analyzing a model successfully calibrated with *in vitro* experimental data for *K. pneumoniae* with phages. We have described a coexistence scenario governed by non-hyperbolic equilibria, opening new avenues to understand the role of these manifolds in real systems. Despite their widespread presence in models of biological systems, these manifolds lack experimental evidence. Future research should also investigate phage-bacteria quasineutral dynamics considering stochasticity. In this sense, previous works described stochastic dynamics as relevant determinants of asymptotic behaviors with quasineutral manifolds [20, 29, 41].

Our results suggest that experimental measurements targeting trajectories along quasineutral manifolds–rather than single equilibrium states–may be crucial for understanding and controlling phage resistance. More broadly, identifying non-hyperbolic dynamical structures in data-driven biological models may reveal hidden constraints on therapeutic optimization that are invisible to purely numerical or equilibrium-based analyses.

Acknowledgements We want to thank the hospitality of the Institute for Integrative Systems Biology and the EnBiVir Lab, which hosted J.A. during the preparation of this manuscript. We also want to thank J. Tomás Lázaro and Mariona Fucho-Rius for their useful comments.

Author Contributions J.S., M.R., P.D-C. developed the mathematical model. J.S. and M.R. performed the fittings of the experimental data. J.A. and F.D. did the mathematical calculations and the numerical investigations. P.D-C. and I.C. designed the experiments and collected the data to build the experimental time series. All authors have participated in the writing of the manuscript.

Funding This work has been funded by projects PID2020- 112835RA-I00 (IC) and PID2023-150309OB-I00 (Spanish Ministry of Science, Innovation, and Universities) funded by MCIN/AEI/10.13039/501100011033 to P.D.-C. Moreover, P.D.-C. was financially supported by a Ramón y Cajal contract RYC2019-028015-I funded by MCIN/AEI/10.13039/501100011033, ESF Invest in your future. F.D. has been supported by the Spanish Research project PID2023-147461NB-I00 funded by AEI. This research has also been funded by the State Research Agency (AEI), through the Severo Ochoa and Maria de Maeztu Program for Centers and Units of Excellence in R&D (CEX2020-001084-M). We thank the CERCA Program/Generalitat de Catalunya for institutional support.

Data Availability No datasets were generated or analysed during the current study.

Declarations

Conflict of interest The authors declare no conflict of interest.

References

1. Collaborators, A.R.: Global burden of bacterial antimicrobial resistance in,: a systematic analysis. Lancet **399**(2022), 629–655 (2019). https://doi.org/10.1016/S0140-6736(21)02724-0
2. Betts, A., Kaltz, O., Hochberg, M.E.: Contrasted coevolutionary dynamics between a bacterial pathogen and its bacteriophages. PNAS **111**, 11109–11114 (2014). https://doi.org/10.1073/pnas.1406763111
3. Campbell, A.: Conditions for the existence of bacteriophage. Evol. **15**, 153–165 (1961). https://doi.org/10.2307/2406076
4. Bernabéu-Gimeno, M., Pardo-Freire, M., Chan, B.K., Turner, P.E., Gil-Brusola, A., Pérez-Tarazona, S., Carrasco-Hernández, L., Quintana-Gallego, E., Domingo-Calap, P.: Neutralizing antibodies after nebulized phage therapy in cystic fibrosis patients. Med **5**, 1096–1111 (2024). https://doi.org/10.1016/j.medj.2024.05.017
5. Bocsó, A., Farkas, M.: Political and economic rationality leads to velcro bifurcation. Appl. Math. Comp. **140**, 381–389 (2003). https://doi.org/10.1016/S0096-3003(02)00235-7
6. Chan, B.K., Turner, P.E., Kim, S., Mojibian, H.R., Elefteriades, J.A., Narayan, D.: Phage treatment of an aortic graft infected with Pseudomonas aeruginosa. Evol. Med. Public Health **2018**, 60–66 (2018). https://doi.org/10.1093/emph/eoy005
7. Chao, L., Levin, B.R., Stewart, F.M.: A complex community in a simple habitat: an experimental study with bacteria and phage. Ecol. **58**, 369–378 (1977). https://doi.org/10.2307/1935611
8. Citorik, R.J., Mimee, M., Lu, T.K.: Sequence-specific antimicrobials using efficiently delivered RNA-guided nucleases. Nat. Biotechnol. **32**, 1141–1145 (2014). https://doi.org/10.1038/nbt.3011
9. Comeau, A.M., Tétart, F., Trojet, S.N., Prère, M.F., Krisch, H.M.: Phage-antibiotic synergy (PAS): β-Lactam and quinolone antibiotics stimulate virulent phage growth. PLoS ONE **2**, 799 (2007). https://doi.org/10.1371/journal.pone.0000799
10. Dedrick, R.M., Guerrero-Bustamante, C.A., Garlena, R.A., Russell, D.A., Ford, K., Harris, K., Gilmour, K.C., Soothill, J., Jacobs-Sera, D., Schooley, R.T., Hatfull, G.F., Spencer, H.: Engineered bacteriophages for treatment of a patient with a disseminated drug-resistant Mycobacterium abscessus. Nat. Med. **25**, 730–733 (2019). https://doi.org/10.1038/s41591-019-0437-z
11. Dedrick, R.M., Smith, B.E., Cristinziano, M., Freeman, K.G., Jacobs-Sera, D., Belessis, Y.W., Brown, Y., Cohen, K.A., van Davidson, R.M., Duin, D., Gainey, A.B., Garcia, C., George, C.R.R., Haidar, G., Ip, W., Iredell, J., Khatami, A., Little, J.S., Malmivaara, K., McMullan, B.J., Michalik, D.E., Moscatelli, A., Nick, J.A.T., Otiz, M.G., Polenakovik, H.M., Robinson, P.D., Skurnik, M., Solomon, D.A., Soothill, J., Spencer, H., Wark, P., Worth, A., Schooley, R.T., Benson, C.A., Hatfull, G.F.: Phage therapy of Mycobacterium infections: compassionate-use of phages in twenty patients with drug-resistant mycobacterial disease. Clin. Infect. Dis. **76**(2023), 103–112 (2023). https://doi.org/10.1093/cid/ciac453
12. Dennehy, J.J.: What can phages tell us about host-pathogen coevolution? Int. J. Evol. Biol. **2012**, 396165 (2012). https://doi.org/10.1155/2012/396165
13. Eskenazi, A., Lood, C., Wubbolts, J., Hites, M., Balarjishvili, N., Leshkasheli, L., Askilashvili, L., Kvachadze, L., van Noort, V., Wagemans, J., Jayankura, M., Chanishvili, N., de Boer, M., Nibbering, P., Kutateladze, M., Lavigne, R., Merabishvili, M., Pirnay, J.P.: Combination of pre-adapted bacteriophage therapy and antibiotics for treatment of fracture-related infection due to pandrug-resistant Klebsiella pneumoniae. Nat. Commun. **13**, 302 (2022). https://doi.org/10.1038/s41467-021-27656-z
14. Farkas, M.: Zip bifurcation in a competition model. Nonlinear Anal. Theory Methods Appl. **8**, 1295–1309 (1984). https://doi.org/10.1016/0362-546X(84)90017-8
15. Farkas, M., Sáez, E., Szántó, I.: Velcro bifurcation in competition models with generalized Holling functional response, Miskolc Math. Notes **6**, 185–195 (2005). https://doi.org/10.18514/MMN.2005.115
16. Ferreira, J.D., de Oliveira, L.A.F.: Zip bifurcation in a competitive system with diffusion. Diff. Eq. Dyn. Sys. **17**, 37–53 (2009). https://doi.org/10.1007/s12591-009-0003-0
17. Ferriol-González, C., Concha-Eloko, R., Bernabéu-Gimeno, M., Fernández-Cuenca, F., Cañada-García, J.E., García-Cobos, S., Sanjuán, R., Domingo-Calap, P.: Targeted phage hunting to specific Klebsiella pneumoniae clinical isolates is an efficient antibiotic resistance and infection control strategy. Microbiol. Spectr. **12**, 00254 (2024). https://doi.org/10.1128/spectrum.00254-24
18. Fontich, E., Guillamon, A., Lázaro, J.T., Alarcón, T., Vidiella, B., Sardanyés, J.: Critical slowing down close to a global bifurcation of a curve of quasi-neutral equilibria. Commun. Nonlinear Sci. Numer. Simul. 104, 106032 (2022). https://doi.org/10.1016/j.cnsns.2021.106032
19. Jennes, S., Merabishvili, M., Soentjens, P., Pang, K.W., Rose, T., Keersebilck, E., Soete, O., François, P.M., Teodorescu, S., Verween, G., De Vos, D., Pirnay, J.P.: Use of bacteriophages in the treatment of colistin-only-sensitive Pseudomonas aeruginosa septicaemia in a patient with acute kidney injury—a case report. Crit. Care **21**, 129 (2017). https://doi.org/10.1186/s13054-017-1709-y
20. Kogan, O., Khasin, M., Meerson, B., Schneider, D., Myers, C.R.: Two-strain competition in quasineutral stochastic disease dynamics. Phys. Rev. E **90**, 042149 (2014). https://doi.org/10.1103/PhysRevE.90.042149
21. Kortright, K.E., Chan, B.K., Koff, J.L., Turner, P.E.: Phage therapy: a renewed approach to combat antibiotic-resistant bacteria. Cell

Host Microbe **25**, 219–232 (2019). https://doi.org/10.1016/j.chom.2019.01.014
22. Koskella, B., Brockhurst, M.A.: Bacteria-phage coevolution as a driver of ecological and evolutionary processes in microbial communities. FEMS Microbiol. Rev. **38**, 916–931 (2014). https://doi.org/10.1111/1574-6976.12072
23. LaSalle, J.: Some Extensions of Liapunov's Second Method. IRE Trans. Circuit Theory **7**, 520–527 (1960). https://doi.org/10.1109/TCT.1960.1086720
24. Kovacs, C.J., Rapp, E.M., Rankin, W.R., McKenzie, S.M., Brasko, B.K., Hebert, K.E., Bachert, B.A., Kick, A.R., Burpo, F.J., Barnhill, J.C.: Combinations of bacteriophage are efficacious against multidrug-resistant Pseudomonas aeruginosa and enhance sensitivity to carbapenem antibiotics. Viruses **16**, 1000 (2024). https://doi.org/10.3390/v16071000
25. Leclerc, Q.J., Lindsay, J.A., Knight, G.M.: Modeling the synergistic effect of bacteriophage and antibiotics on bacteria: killers and drivers of resistance evolution. PLoS Comput. Biol. **18**, 1010746 (2022). https://doi.org/10.1371/journal.pcbi.1010746
26. Lenski, R.E.: Coevolution of bacteria and phage: are there endless cycles of bacterial defenses and phage counter-defenses? J. Theor. Biol. **108**, 319–325 (1984). https://doi.org/10.1016/S0022-5193(84)80035-1
27. Leung, C.Y.J., Weitz, J.S.: Modeling the synergistic elimination of bacteria by phage and the innate immune system. J. Theor. Biol. **429**, 241–252 (2017). https://doi.org/10.1016/j.jtbi.2017.06.037
28. Levin, B.R., Stewart, F.M., Chao, L.: Resource-limited growth, competition, and predation: a model and experimental studies with bacteria and bacteriophage. Am. Nat. **111**, 3–24 (1977). https://doi.org/10.1086/283134
29. Lin, Y.T., Kim, H., Doering, C.R.: Features of fast living: on the weak selection for longevity in degenerate birth-death processes. J. Stat. Phys. **148**, 647–663 (2012). https://doi.org/10.1007/s10955-012-0479-9
30. Luo, J., Xie, L., Liu, M., Li, Q., Wang, P., Luo, C.: Bactericidal synergism between phage YC#06 and antibiotics: a combination strategy to target multidrugresistant Acinetobacter baumannii in vitro and in vivo. Microbiol. Spectr. 10(4):e0009622 (2022). https://doi.org/10.1128/spectrum.00096-22
31. Mukhopadhyay, S., Zhang, P., To, K.K.W., Liu, Y., Bai, C., Leung, S.S.Y.: Sequential treatment effects on phage-antibiotic synergistic application against multidrug-resistant Acinetobacter baumannii. Int. J. Antimicrob. Agents **62**, 106951 (2023). https://doi.org/10.1016/j.ijantimicag.2023.106951
32. Muñoz-Sánchez, J.C., Lázaro, J.T., Hillung, J., Olmo-Uceda, M.J., Sardanyés, J., Elena, S.F.: Quasineutral multistability in an epidemiological-like model for defective-helper betacoronavirus infection in cell cultures. Appl. Math. Model. **137**, 115673 (2025). https://doi.org/10.1016/j.apm.2024.115673
33. Naga, N.G., Shaaban, M.I., El-Metwally, M.M.: An insight on the powerful of bacterial quorum sensing inhibition. Eur. J. Clin. Microbiol. Infect. Dis. **43**, 2071–2081 (2024). https://doi.org/10.1007/s10096-024-04920-w
34. Oechslin, F., Piccardi, P., Mancini, S., Gabard, J., Moreillon, P., Entenza, J.M., Resch, G., Que, Y.A.: Synergistic interaction between phage therapy and antibiotics clears Pseudomonas aeruginosa infection in endocarditis and reduces virulence. J. Infect. Dis. **215**, 703–712 (2017). https://doi.org/10.1093/infdis/jiw632
35. Pardo-Freire, M. Domingo-Calap, P.: Phages and nanotechnology: new insights against multidrug-resistant bacteria, Biodes. Res. 5 (2023). https://doi.org/10.34133/bdr.0004
36. Ranveer, S.A., Dasriya, V., Ahmad, M.F., Dhillon, H.S., Samtiya, M., Shama, E., Anand, T., Dhewa, T., Chaudhary, V., Chaudhary, P., Behare, P., Ram, C., Puniya, D.V., Khedkar, G.D., Raposo, A., Han, H., Puniya, A.K.: Positive and negative aspects of bacteriophages and their immense role in the food chain, npj Sci. Food **8**, 1 (2024). https://doi.org/10.1038/s41538-023-00245-8
37. Rodríguez, M. Cantallops, I. Domingo-Calap, P. Sardanyés, J. :Rodríguez, M. Cantallops, I. Domingo-Calap, P. Sardanyés, J.: Quantifying phage-bacteria dynamics in vitro: rapid emergence of phage-resistant mutants for Klebsiella pneumoniae. microPublication Biology (2025) https://doi.org/10.17912/micropub.biology.001666
38. Fiedler, B. Liebscher, S.: Bifurcations without parameters: some ODE and PDE examples. arXiv:math/0304453 (2003)
39. Fiedler, B., Liebscher, S., Alexander, J.C.: Generic Hopf bifurcation from lines of equilibria without parameters: I. Theory. J. Diff. Equ. **167**, 16–35 (2000). https://doi.org/10.1006/jdeq.2000.3779
40. Rodriguez-Gonzalez, R.A., Leung, C.Y.J., Chan, B.K., Turner, P.E., Weitz, J.S.: Quantitative models of phage-antibiotic combination therapy. mSystems **5**, 00756 (2020). https://doi.org/10.1128/msystems.00756-19
41. Sardanyés, J., Arderiu, A., Elena, S.F., Alarcón, T.: Noise-induced bistability in the quasineutral coexistence of viral RNA under different replication modes. J. R. Soc. Interface **15**, 20180129 (2018). https://doi.org/10.1098/rsif.2018.0129
42. Schooley, R.T., Biswas, B., Gill, J.J., Hernandez-Morales, A., Lancaster, J., Lessor, L., Barr, J.J., Reed, S.L., Rohwer, F., Benler, S., Segall, A.M., Taplitz, R., Smith, D.M., Kerr, K., Kumaraswamy, M., Nizet, V., Lin, L., McCauley, M.D., Strathdee, S.A., Benson, C.A., Pope, R.K., Leroux, B.M., Picel, A.C., Mateczun, A.J., Cilwa, K.E., Regeimbal, J.M., Estrella, L.A., Wolfe, D.M., Henry, M.S., Quinones, J., Salka, S., Bishop-Lilly, K.A., Young, R., Hamilton, T.: Development and use of personalized bacteriophage-based therapeutic cocktails to treat a patient with a disseminated resistant Acinetobacter baumannii infection. Antimicrob. Agents Chemother. **61**, 00954 (2017). https://doi.org/10.1128/aac.00954-17
43. Strathdee, S.A., Hatfull, G.F., Mutalik, V.K., Schooley, R.T.: Phage therapy: from biological mechanisms to future directions. Cell **186**, 17–31 (2023). https://doi.org/10.1016/j.cell.2022.11.017
44. Weitz, J.S.: Quantitative viral ecology: dynamics of viruses and their microbial hosts, Princeton University Press, Princeton (2015). https://doi.org/10.23943/princeton/9780691161549.001.0001